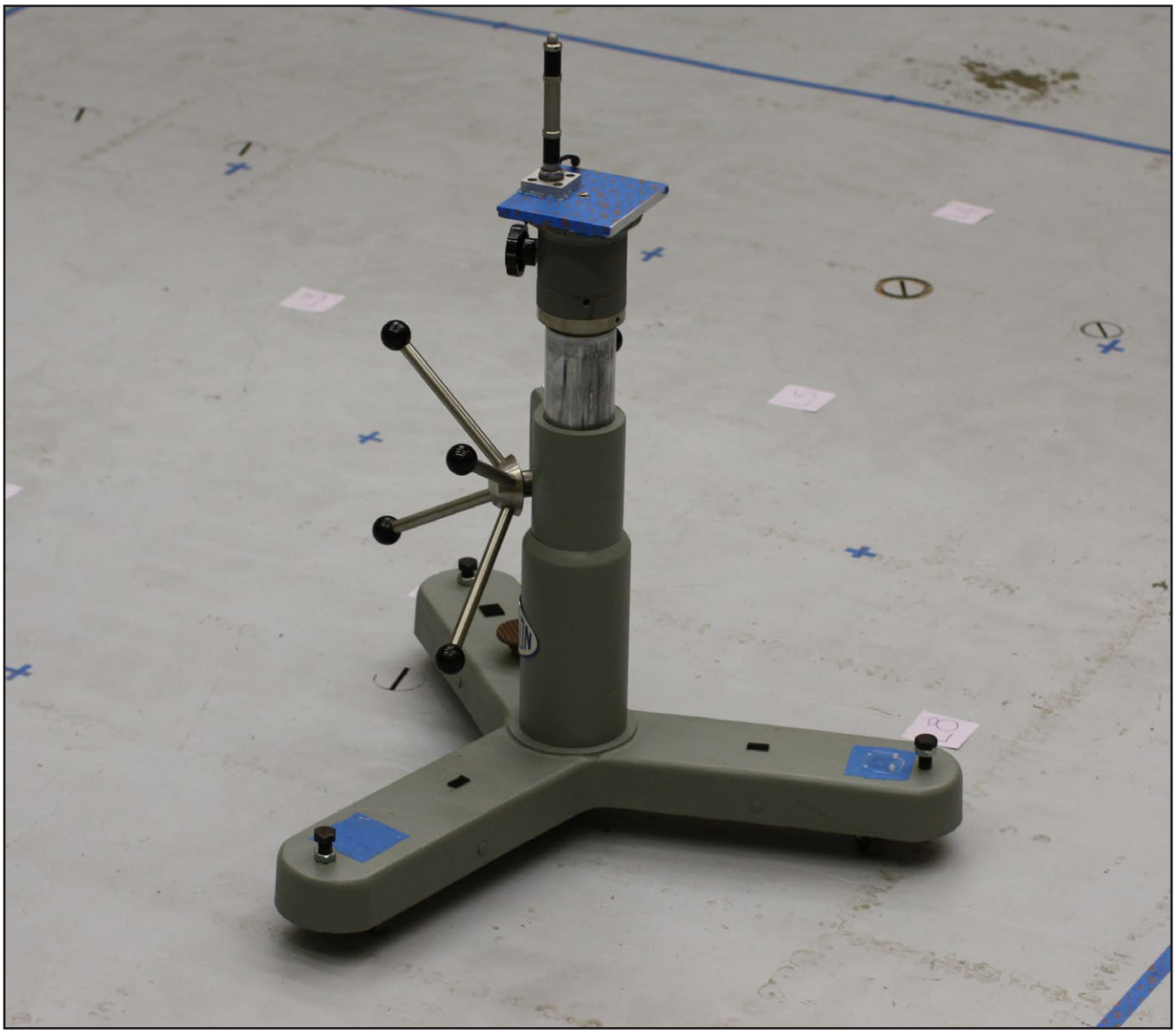

Precision vs. Accuracy Dilemma in Point-Based Rigid-Body Registration

by Marek Franaszek and Geraldine Cheok, NIST

The purpose of a registration procedure is to determine the transformation between two coordinate frames: the working frame (from which 3D data are transformed) and the destination frame (to which the data are transformed). In point-based, rigid-body registration, the transformation is calculated from measurements of the same physical points acquired in both frames. These two sets of corresponding points are called fiducials, and the quality of registration is frequently gauged by the root mean square (RMS) of distances between the fiducials measured in the destination frame and corresponding fiducials transformed from the working frame. However, in practical applications another metric is more useful: RMS of distances between targets measured in the destination frame and the corresponding targets transformed from the working frame. Targets are points to which registration transformation is applied, but they are not used to calculate the parameters of the transformation. Thus, smaller target's RMS would correspond to a more accurate registration. Noisy measurements of fiducials in both frames yield noisy registration parameters, and they cause the uncertainty of the target

point transformed to the destination frame to be larger than the uncertainty of the target measured in the working frame. The increased uncertainty of transformed targets can be used as a measure of registration precision: Smaller increases correspond to more precise registrations.

In this article, we show that the precision and accuracy of the registration depend on the location of the fiducials for the general case where the noise is nonhomogeneous, anisotropic, and the 3D data contain a bias. The obtained experimental results indicate that the configuration of fiducials that yields a more accurate registration does not necessarily yield a registration that has a small uncertainty, and vice versa: The configuration that yields small uncertainties of the transformed targets does not necessarily result in accurate registration.

INTRODUCTION

Registration is required when some 3D points are acquired in one coordinate frame but need to be accessed in another frame. Then, the rigid-body transformation (rotation $\boldsymbol{R}$ and translation τ) is needed to transform points measured in the working frame to the destination frame. The sought transformation minimizes the following error function RMS_F:

$$RMS_F(\{\boldsymbol{X}\}_N, \{\boldsymbol{Y}\}_N) = min\sqrt{\left(\frac{1}{N}\sum_{n=1}^{N}\|\boldsymbol{R}\boldsymbol{X}_n + \boldsymbol{\tau} - \boldsymbol{Y}_n\|^2\right)} \quad \text{(Equation 1)}$$

where $\{\boldsymbol{X}\}_N$ is a set of N fiducial points measured in the working frame and $\{\boldsymbol{Y}\}_N$ is the set of corresponding fiducials measured in the destination frame. The definition of such error function is based on the rigid-body assumption: The distance between any two points measured in the working frame should be equal to the distance between the same two points measured in the destination frame:

$$\| \boldsymbol{X}_n - \boldsymbol{X}_m \| = \|\boldsymbol{Y}_n - \mathrm{Y}_m \| \quad \text{(Equation 2)}$$

Due to noise and bias of the measured 3D points, equation 2 does not hold, and the least-square fitting procedure is used to solve the minimization problem seen in equation 1. It seems natural to interpret the residual value of the error function as a metric for the quality of registration. However, there are two types of problems that put in doubt the usefulness of this metric. The first type of problem is associated with the fundamental characteristics of each measurement: accuracy and uncertainty. Quantification of accuracy is based on the difference between the measurand and ground truth. However, the ground-truth measurements (three angles of rotation $\boldsymbol{R}$ and three components of translation vector τ) are generally not available: Even if a better instrument is used to measure the locations of fiducials, in most cases it cannot be placed in the exact same location as the instrument under test.

The second type of problem is associated with the actual use of registration transformation. Once the registration is performed, the transformation is applied to the target points, i.e., points that were not used in the registration procedure but which are points of interest to the user. Then, the target registration error RMS_T is defined as:

$$RMS_T(\{\boldsymbol{T}_X\}_K, \{\boldsymbol{T}_Y\}_K) = \sqrt{\frac{1}{K}\sum_{k=1}^{K}\left\|\boldsymbol{R}\boldsymbol{T}_{X,k} + \boldsymbol{\tau} - \boldsymbol{T}_{Y,k}\right\|^2} \quad \text{(Equation 3)}$$

where $\{\boldsymbol{T}_X\}_K$ is a set of K target points in the working frame and $\{\boldsymbol{T}_Y\}_K$ is a set of corresponding targets in the destination frame. Also, it has been demonstrated (and experimental results presented in this article support the finding) that RMS_F increases with the number of fiducials N used in the registration.[1,2] This is a rather surprising finding as a better fit of the model is expected for a larger number of experimental points for most least-squared minimization problems. Because of this counterintuitive finding, the use of RMS_F as the metric for the quality of registration may be misleading. In contrast, RMS_T *decreases* with the number of fiducials N for a given set of K targets.

In many practical applications where the targets $\{\boldsymbol{T}_Y\}_K$ in the destination frame are not measured, RMS_T in equation 3 cannot be calculated (i.e., if the targets in the destination frame could be measured, then there would be no need to perform a registration). Without a reliable gauge of registration performance, it is impossible to answer questions such as, "How many fiducials should be used for registration, and where should they be placed in the work volume?"[3–8]

To address these questions, there has been much effort made to create an analytical formula that could express the target registration error as a function of measurable features, such as fiducial locations $\{\boldsymbol{X}\}_N$, $\{\boldsymbol{Y}\}_N$, target locations $\{\boldsymbol{T}_X\}_K$ in the working frame, and their corresponding noise characteristics (covariance matrixes). Depending on the complexity of the noise models for the fiducials, different analytical formulas have been developed.[9–13] The first,[2] based on a zero-mean Gaussian noise distribution with fixed variance s^2 (the same covariance matrix at each fiducial location equal to $s^2\boldsymbol{I}_{3\times3}$) yielded the following prediction for the mean registration error of a single target $TRE(\boldsymbol{T}_X)$:

$$TRE(\boldsymbol{T}_X) \approx s\sqrt{\frac{1}{N}\left(1 + \frac{1}{3}\sum_{j=1}^{3}\left(d_j/f_j\right)^2\right)}, \quad \text{(Equation 4)}$$

where d_j is the distance of the target $\boldsymbol{T}_X$ from the j-th principal axis and f_j is the RMS distance of the N fiducials from the j-th principal axis (the axes are determined from the singular value decomposition (SVD) of the covariance matrix of the fiducial locations). TRE in equation 4 has two components. The first component (independent of target location $\boldsymbol{T}_X$) is associated with the uncertainty of the translation τ; the second term depends on the target's location relative to the fiducials, and it has anisotropic dependence. The second component is associated with uncertainty of rotation $\boldsymbol{R}$. Subsequent, more advanced models of noise led to more complex versions of equation 4, but the existence of bias in the measured fiducial and target locations have not been properly addressed thus far.[14]

The above considerations led to the following idea: Instead of relying on the usually unavailable errors of the six registration parameters, it would be more useful to gauge the performance of registration in an operational sense by asking, "How good is the outcome of transformation of target points?"

Based on this concept, three versions of RMS_T as defined in equation 3 are calculated. In this study, repeated measure-

ments of fiducial and target locations in the same experimental conditions were obtained, and targets were measured in both frames: working and destination. For each i-th repeat measurement of the fiducials $\{\boldsymbol{X}\}_{N,i}$ and $\{\boldsymbol{Y}\}_{N,i}$, the corresponding registration transformation $\{\boldsymbol{R}_i, \tau_i\}$ is found by minimizing equation 1 and calculating the corresponding residual value of the error function $RMS_{F,i}$. Then, for each i-th registration, the following metrics based on target locations are calculated:

$$RMS_{C,i}(\{\langle \boldsymbol{T}\rangle_X\}_K, \{\langle \boldsymbol{T}\rangle_Y\}_K) = \sqrt{\frac{1}{K}\sum_{k=1}^{K}\left\|\boldsymbol{R}_i\langle \boldsymbol{T}\rangle_{X,k} + \boldsymbol{\tau}_i - \langle \boldsymbol{T}\rangle_{Y,k}\right\|^2} \quad \text{(Equation 5)}$$

$$RMS_{G,i}(\{\boldsymbol{T}_X\}_{K,i}, \{\boldsymbol{T}_Y\}_{K,i}) = \sqrt{\frac{1}{K}\sum_{k=1}^{K} TRE_i^2(\boldsymbol{T}_k)} \quad \text{(Equation 6)}$$

$$RMS_{U,i}(\{\boldsymbol{T}_X\}_{K,i}) = \sqrt{\frac{1}{K}\sum_{k=1}^{K}\left\|\tilde{\boldsymbol{T}}_{X,k,i} - \langle \tilde{\boldsymbol{T}}_{X,k,i}\rangle\right\|^2} \quad \text{(Equation 7)}$$

where $\tilde{\boldsymbol{T}}_{X,k,i}$ is the i-th instance of the k-th target transformed from the working to the destination frame by i-th transformation $\{\boldsymbol{R}_i, \tau_i\}$ as follows:

$$\tilde{\boldsymbol{T}}_{X,k,i} = \boldsymbol{R}_i\, \boldsymbol{T}_{X,k,i} + \tau_i \quad \text{(Equation 8)}$$

and

$$TRE_i\,(\boldsymbol{T}_k) = \| \tilde{\boldsymbol{T}}_{X,k,i} - \boldsymbol{T}_{Y,k,i} \| \quad \text{(Equation 9)}$$

is the error of the individual k-th target transformed by the i-th transformation.

The averaged target locations $\{\langle \boldsymbol{T}\rangle_X\}_K$ and $\{\langle \boldsymbol{T}\rangle_Y\}_K$ are used in equation 5; instantaneous, i-th target locations $\{\boldsymbol{T}_X\}_{K,i}$ and $\{\boldsymbol{T}_Y\}_{K,i}$ measured in both frames are used in equation 6; and only $\{\boldsymbol{T}_X\}_{K,i}$ measured in the working frame are used in equation 7. Thus, $RMS_{C,i}$ gauges the error of registration caused by possible bias (in fiducials and targets locations) and noise of the fiducials only while $RMS_{G,i}$ is more general as it depends on bias and noise in both fiducials and targets; therefore, $RMS_{G,i}$ is expected to have larger variation than $RMS_{C,i}$ Then, the mean $\langle RMS_C\rangle$, $\langle \mathrm{RMS}_G\rangle$, and $\langle RMS_U\rangle$ are calculated together with the corresponding standard deviations σ_C, σ_G, and σ_U.

For comparison, the mean of residual values of the error function $\langle \mathrm{RMS}_F\rangle$ is also evaluated. The accuracy of registration as gauged by $\langle \mathrm{RMS}_C\rangle$ or $\langle \mathrm{RMS}_G\rangle$ cannot be determined in most practical applications as it requires the measurement of targets in the destination frame. Calculation of $\langle \mathrm{RMS}_U\rangle$ is possible in most applications as it does not require measurement of targets in the destination frame, and it is a measure of registration uncertainty. $\langle \mathrm{RMS}_C\rangle$, $\langle \mathrm{RMS}_G\rangle$, and $\langle \mathrm{RMS}_U\rangle$ depend on the location of fiducials in the work volume. We show that the configuration of fiducials that yields small $\langle \mathrm{RMS}_U\rangle$ does not necessarily yield small $\langle \mathrm{RMS}_C\rangle$ or $\langle \mathrm{RMS}_G\rangle$. The set of fiducials yielding the optimum accuracy may not yield optimum precision and vice versa.

In the next section, a brief description of the experimental setup and data collection is provided. Then, data post-processing is outlined followed by presentation of the results. The final section contains a discussion and conclusions.

EXPERIMENT

The data (locations of 3D points) were acquired using three different instruments: System A (a motion-capture system based on a network of 2D cameras), System B (a large-scale metrology indoor positioning system), and a laser tracker. System A had low noise and large bias, System B had higher noise relative to System A and very small bias, and the laser tracker had very low noise and no bias. In the work volume (3 m × 3 m × 1.8 m), 125 points were distributed on a semi-regular 5 × 5 × 5 grid. In addition to these points, a set of 16 points, randomly distributed in the work volume, was acquired by the three instruments. Different configurations of N points were selected from the 125 grid points as fiducials for registrations, and the 16 irregularly scattered points were used as targets to which registration transformations were applied. Each fiducial and target point was measured 200 times by Systems A and B (no repeats were acquired by the laser tracker because this instrument was considered noise and bias-free for the purposes of this study). The acquired data enabled registration between three pairs of instruments (A to B, A to the laser tracker, and B to the laser tracker). Calibration of Systems A and B, as described in the user's manuals, was performed before the data collection had started. However, individual cameras in System A were not calibrated, and filtering of streamed data in System B was turned off during data collection.

DATA POST-PROCESSING AND RESULTS

From 200 repeated measurements, the mean location and the covariance matrix for each fiducial and target point were calculated. The mean locations were used to check the rigid-body assumption for registering the working frame to the destina-

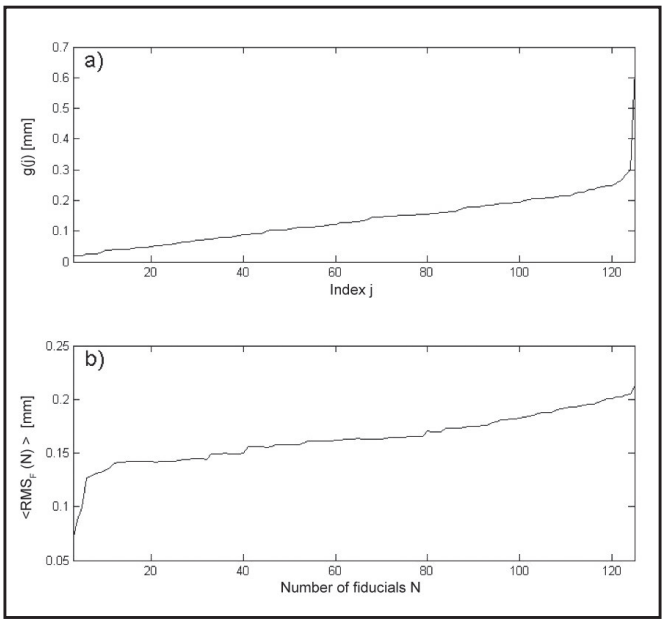

Figure 1. *a) Parameter g(j) and b) the mean* $\langle \mathrm{RMS}_F(N)\rangle$ *for data acquired by System B and the laser tracker; also, the selection of* N = j *fiducials seen in b) is based on the list of ordered* g(j) *as seen in a)*

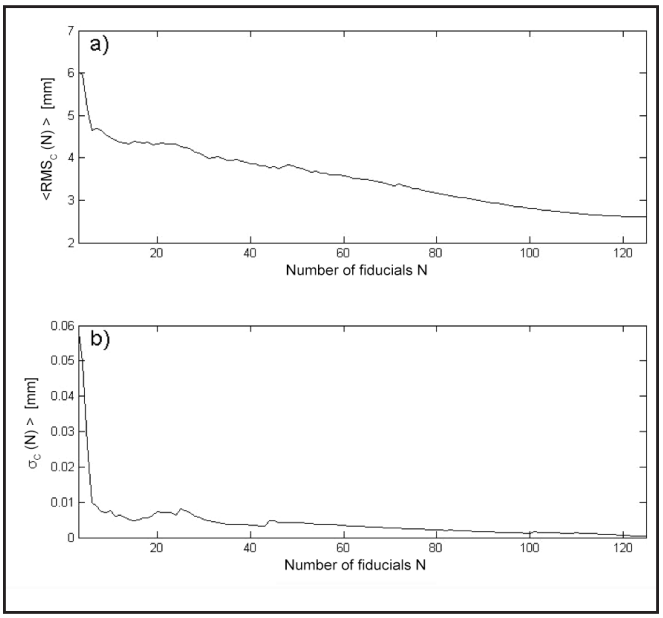

Figure 2. a) Mean ⟨RMS$_C$ (N)⟩; b) σ_C for data acquired with System A and laser tracker

tion frame. For that purpose, the distance between two points ($\langle \boldsymbol{Y} \rangle_n, \langle \boldsymbol{Y} \rangle_m$) measured in the destination frame was compared with the distance between the same two points measured in the working frame ($\langle \boldsymbol{X} \rangle_n, \langle \boldsymbol{X} \rangle_m$). The difference between the distances is:

$$L_{n,m} = \| \langle \boldsymbol{X} \rangle_n - \langle \boldsymbol{X} \rangle_m \| - \| \langle \boldsymbol{Y} \rangle_n - \langle \boldsymbol{Y} \rangle_m \| \qquad \text{(Equation 10)}$$

A large absolute value $|L_{n,m}|$ indicates that the rigid-body assumption is poorly satisfied. For all three pairs of instruments (Systems A and B, A and the laser tracker, B and the laser tracker), the smallest $| L_{n0,m0} |$ was found out of all possible $| L_{n,m} |$ determined for fiducials, and the parameter $g(j)$ was calculated as:

$$g(j) = (|L_{j,n0}| + | L_{j,m0} |)/2 \qquad \text{(Equation 11)}$$

where $j \neq n0, m0$. By sorting $g(j)$ in ascending order, points with large $g(j)$ could be identified, and these points would be bad candidates for registration. A series of registrations for a decreasing number of N fiducials was performed. The first iteration started with the full set of $M = 125$ grid points selected as N fiducials, and for 200 repeat measurements of fiducials $\{\boldsymbol{X}\}_{N,i}$ and $\{\boldsymbol{Y}\}_{N,i}$ ($i \leq 200$), the corresponding registration transformations $\{\boldsymbol{R}_i, \tau_i\}$ were determined. For each registration, fiducial registration error $RMS_{F,i}$ and targets error $RMS_{C,i}$ were calculated. From the 200 values, the mean values $\langle RMS_F \rangle$, $\langle RMS_C \rangle$ and the standard deviation σ_C were then calculated. The next iteration used $N - 1$ fiducials, after removing the point with the largest parameter $g(j)$, to perform the new registration, and $\langle RMS_F \rangle$, $\langle RMS_C \rangle$, and σ_C were recalculated. The iterative process was continued until the minimum number of fiducials $N = 3$ was reached. This

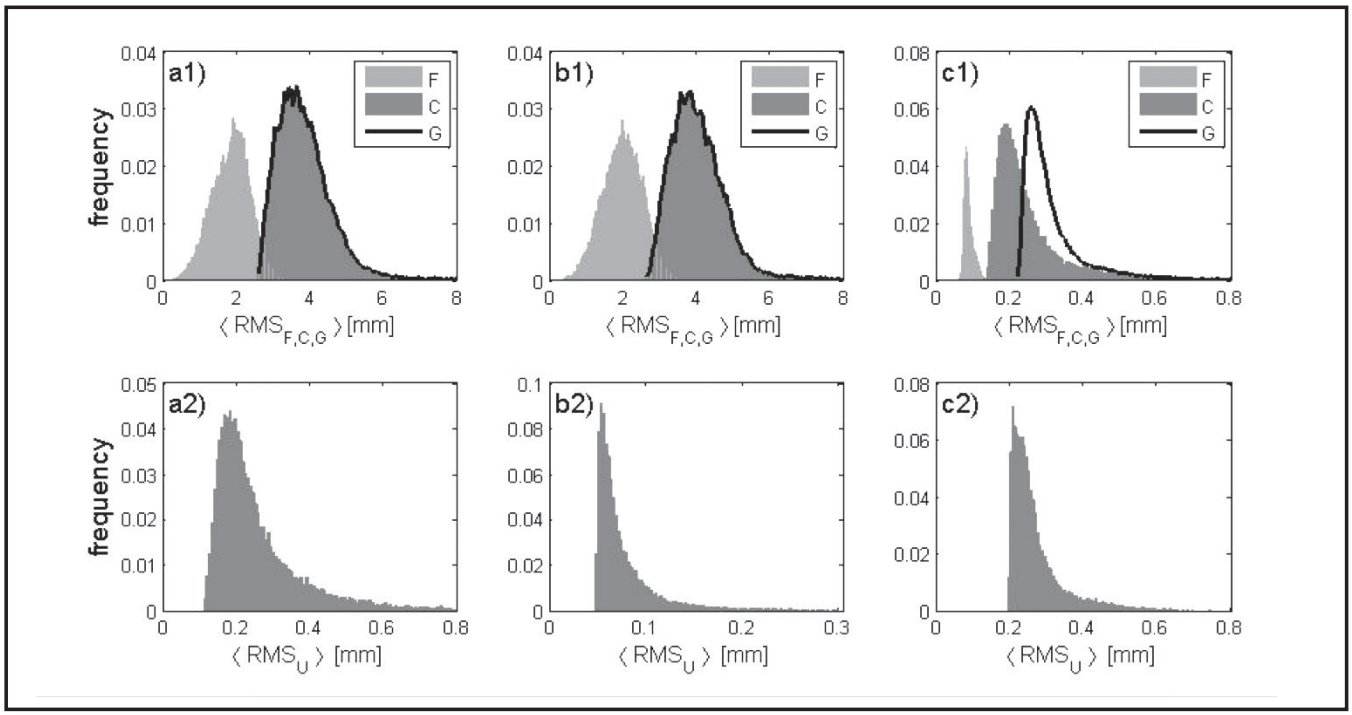

Figure 3. Histograms of four mean characteristics for registrations using all possible triplets of fiducials from a limited pool of grid points; plots in column: a) for registering System A to B; b) System A to laser tracker; c) System B to laser tracker; upper row: ⟨RMS$_F$⟩, ⟨RMS$_C$⟩, and ⟨RMS$_G$⟩; lower row: ⟨RMS$_U$⟩

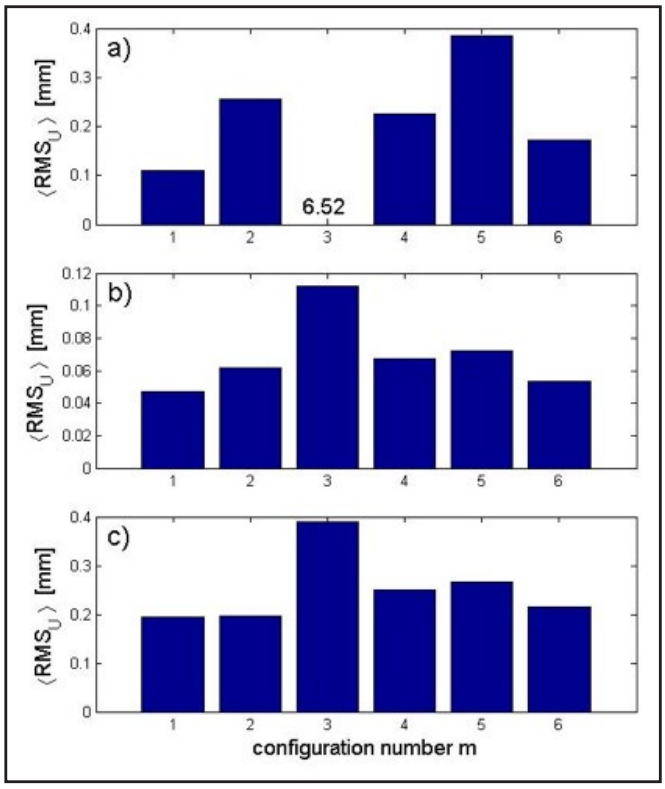

Figure 4. Mean ⟨RMS$_U$⟩ for registrations based on six different N = 3 fiducials, yielding the: 1) smallest ⟨RMS$_U$⟩ ; 2) smallest ⟨RMS$_C$⟩; 3) smallest ⟨RMS$_F$⟩; 4) median ⟨RMS$_U$⟩; 5) median ⟨RMS$_C$⟩; 6) median ⟨RMS$_F$⟩; registrations were for: a) System A to B; b) System A to laser tracker; c) System B to laser tracker; for m = 3 in a), ⟨RMS$_U$⟩ is much larger, and its numerical value is provided instead

last triplet of fiducials contains fiducials ($n0$, $m0$) for which $|L_{(n0,m0)}|$ is the smallest, and the third fiducial $k0$ for which $g(k0)$ is the smallest. Figure 1 shows example results for data acquired with System B and the laser tracker. Figure 1a shows $g(j)$, and figure 1b shows the mean $\langle RMS_F(N)\rangle$ where N is the number of fiducials used for registration and is based on $g(j)$.

For example, for $N = 3$, the fiducials used are $n0$ and $m0$, and the point corresponding to the smallest $g(j)$; for $N = 4$, the same fiducials as for $N = 3$ and the point corresponding to the next smallest $g(j)$ are used. The plots for System A to the laser tracker and System A to System B yield similar characteristics and are not shown.

Figure 2 shows the results for registering System A to the laser tracker. Figure 2a shows the mean $\langle RMS_C(N)\rangle$, and figure 2b shows standard deviation $\sigma_C(N)$. Registration of System B to the laser tracker and System A to System B yield similar plots.

Registrations using all possible triplets of fiducials selected from a limited pool of grid points were also performed. The pool was limited to the first 60 grid points ordered according to an increasing value of parameter $g(j)$. For 60 points, the total possible number of triplets is equal to $\binom{60}{3} = 34{,}220$. For each triplet, the mean values $\langle RMS_F\rangle$, $\langle RMS_C\rangle$, $\langle RMS_G\rangle$, $\langle RMS_U\rangle$, and the standard deviations of these values, were determined. The histograms of these values were then plotted and can be seen in figure 3.

From the 34,220 values calculated for each metric, fiducials ($N = 3$) corresponding to the smallest and the median values (rank = 1 and 34,220/2 on an ascending list of values) were identified. Figure 4 shows values of $\langle RMS_U\rangle$ determined for the six different $N = 3$ configurations where the first three bars correspond to the configuration yielding the smallest values of $\langle RMS_U\rangle$, $\langle RMS_C\rangle$, and $\langle RMS_F\rangle$, and the last three correspond to the configuration yielding median values of $\langle RMS_U\rangle$, $\langle RMS_C\rangle$, and $\langle RMS_F\rangle$. Similar plots for $\langle RMS_U\rangle$, $\langle RMS_C\rangle$ can be seen in figure 5.

From the repeated measurements of fiducials $\{X\}_{N,i}$ and $\{Y\}_{N,i}$, the corresponding noisy registration transformations $\{\boldsymbol{R}_i,\tau_i\}$ were determined. Then, a regular grid of $M \times L$ points (ϑ_m,φ_l) on a unit sphere was created $(-\pi/(2 \le \vartheta_m \le \pi/2, 0 \le \varphi_l \le 2\pi)$ and for each pair of angles, a corresponding unit vector $\boldsymbol{v}_{m,l}$ was determined as:

$$\boldsymbol{v}_{m,l} = [\cos\vartheta_m \cos\varphi_l\ , \cos\vartheta_m \sin\varphi_l\ , \sin\varphi_l\ ] \qquad \text{(Equation 12)}$$

Then, all 200 noisy rotations were applied to $\boldsymbol{v}_{m,l}$, yielding 200 noisy vectors $\boldsymbol{w}_{m,l,i} = \boldsymbol{R}_i\boldsymbol{v}_{m,l}$, for which the average unit vector $\langle \boldsymbol{w}_{m,l}\rangle$ was calculated. Once the average vector was known, the angles $\alpha_{m,l,i}$ between the i-th and the average vectors were calculated as:

$$\alpha_{m,l,i} = \operatorname{acos}(\boldsymbol{w}_{m,l,i}) \bullet \langle \boldsymbol{w}_{m,l,i}\rangle \qquad \text{(Equation 13)}$$

where • is the dot product of two vectors, and the resulting median angle $\sigma_{m,l}$ was determined. The procedure was repeated for all (ϑ_m,φ_l) points, $m \le M = 180$, and $l \le L = 360$. Thus, $\sigma_{m,l}$ can be viewed as a measure of the angular uncertainty of the transformed target point $\tilde{\boldsymbol{T}}_X(\vartheta_m,\varphi_l) = \boldsymbol{R}_i\,\boldsymbol{T}_X(\vartheta_m,\varphi_l)+\tau_i$.

Then, the average rotation $\boldsymbol{R}_{avg}$ was calculated[15] and the i-th rotation was expressed as a composition of $\boldsymbol{R}_{avg}$ and a small random perturbation $\Delta\boldsymbol{R}_i$, which can be evaluated as:

$$\Delta\boldsymbol{R}_i = \boldsymbol{R}^T_{avg}\,\boldsymbol{R}_i \qquad \text{(Equation 14)}$$

where $\boldsymbol{R}^T_{avg}$ is the transposed matrix of the average rotation. In the axis and angle representation, the smallness of $\Delta\boldsymbol{R}_i(\boldsymbol{a}_i,\rho_i)$ is gauged by the smallness of the rotation angle ρ_i and $\Delta\boldsymbol{R}_i$ in a linear approximation as:

$$\Delta\boldsymbol{R}_i(\boldsymbol{a}_i,\rho_i) \approx \begin{bmatrix} 1 & -q_{z,i} & q_{y,i} \\ q_{z,i} & 1 & -q_{x,i} \\ -q_{y,i} & q_{x,i} & 1 \end{bmatrix},\ \boldsymbol{q}_i = \rho_i\boldsymbol{a}_i\,. \qquad \text{(Equation 15)}$$

Then, the 3 × 3 covariance matrix of rotations $cov(\boldsymbol{q})$ was calculated as:

$$cov(\boldsymbol{q}) = \frac{1}{I}[\bar{\boldsymbol{q}}_1 \cdots \bar{\boldsymbol{q}}_I][\bar{\boldsymbol{q}}_1 \cdots \bar{\boldsymbol{q}}_I]^T \qquad \text{(Equation 16)}$$

where demeaned $\bar{\boldsymbol{q}}_i = \boldsymbol{q}_{ii} - \boldsymbol{q}_{avg}$, eigenvectors $\{\boldsymbol{u}_1, \boldsymbol{u}_2, \boldsymbol{u}_3\}$ and eigenvalues $\{\Lambda_1,\Lambda_2,\Lambda_3\}$ of $cov(\boldsymbol{q})$ were determined.

Figures 6a and 7a show the distributions of the angular uncertainty (expressed as the median angle σ) on a unit sphere together with the directions of the eigenvectors $\{\boldsymbol{u}_1,\boldsymbol{u}_2,\boldsymbol{u}_3\}$. For each unit vector $\boldsymbol{v}_{m,l}$ (ϑ_m,φ_l), the dimensionless coefficient $\gamma_{m,l}$ was calculated as:

$$\gamma^2_{m,l}(\vartheta_m,\varphi_l) = \boldsymbol{v}^T_{m,l}\ \Gamma(\langle X\rangle_N,\langle Y\rangle_N)\ \boldsymbol{v}_{vm,l} \qquad \text{(Equation 17)}$$

where Γ is a 3 × 3 moment of inertia matrix[11] calculated from the mean locations of N fiducials $\langle \boldsymbol{X}\rangle_N$ and $\langle \boldsymbol{Y}\rangle_N$ acquired in the working and destination frame. $\gamma^2_{m,l}$ is proportional to the rotational part of the squared target error seen in equation 4. Figures 6b and 7b show the distribution of γ on a unit sphere.

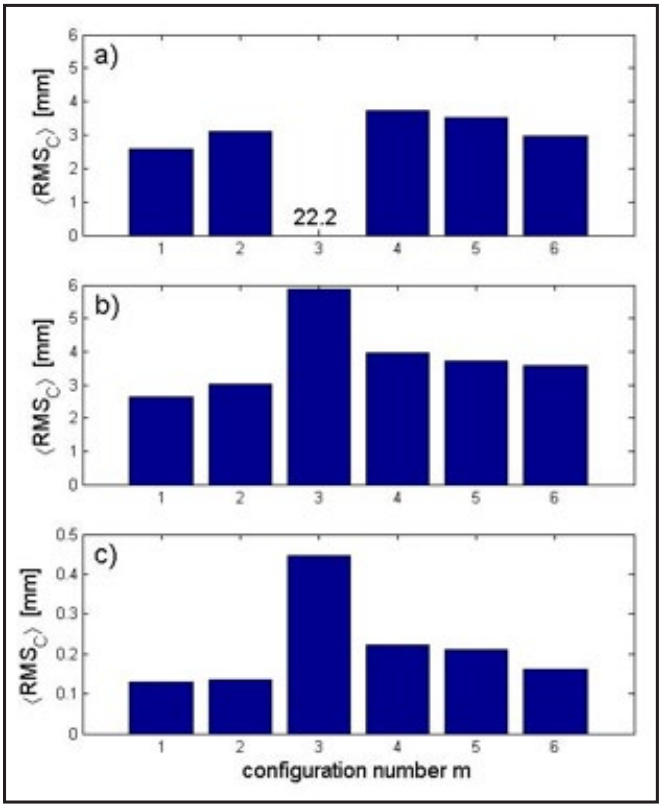

Figure 5. Mean ⟨RMS$_C$⟩ for registrations based on six different N = 3 fiducials, yielding the: 1) smallest ⟨RMS$_C$⟩; 2) smallest ⟨RMS$_U$⟩; 3) smallest ⟨RMS$_F$⟩; 4) median ⟨RMS$_C$⟩; 5) median ⟨RMS$_U$⟩; 6) median ⟨RMS$_F$⟩; registrations were for: a) System A to B; b) System A to laser tracker; c) System B to laser tracker; for m = 3 in a), ⟨RMS$_C$⟩ is much larger, and its numerical value is provided instead

DISCUSSION AND CONCLUSIONS

Figure 1 confirms earlier findings[1,2] that an increasing number N of fiducials used in registration yields larger values of $\langle RMS_F \rangle$. This observation seems to be counterintuitive, but we should recall that fiducials were sorted in order of increasing value of $g(j)$. Thus, consecutive registrations were performed on more and more fiducials of consistently worsening quality. However, for mean target errors $\langle RMS_C \rangle$, a reverse trend is observed as $\langle RMS_C \rangle$, and σ_C decreases with increasing N, as seen in figure 2. Thus, the use of readily available $\langle RMS_F \rangle$ as a metric for registration quality as gauged by usually unavailable $\langle RMS_C \rangle$ may be misleading. This conclusion is also supported by the histograms seen in figure 3: The histograms of $\langle RMS_C \rangle$ are shifted right (larger values) when compared with the histograms of $\langle RMS_F \rangle$. Further evidence is provided in figures 4 and 5: The configurations of $N = 3$ fiducials that yielded the smallest $\langle RMS_F \rangle$ (configuration $m = 3$), yielded very large $\langle RMS_C \rangle$ and $\langle RMS_U \rangle$.

In figures 4 and 5, the triplet of fiducials that yielded the smallest $\langle RMS_C \rangle$ (configuration $m = 2$ in figure 4) does not necessarily lead to the smallest $\langle RMS_U \rangle$. Similarly, the triplet of fiducials that generates the smallest $\langle RMS_U \rangle$ (configuration $m = 2$ in figure 5) does not generate the smallest $\langle RMS_C \rangle$. For $m = 1$ and $m = 2$, the differences between $\langle RMS_U \rangle$ in figures 4c and $\langle RMS_C \rangle$ in figure 5c are smaller than the corresponding differences in figures 4 (a,b) and 5 (a,b). These differences may be caused by the different characteristics of Systems A and B: Average noise for A is almost three times smaller than for B (0.059 mm vs 0.163 mm).[16] The bias (gauged by the average error $L_{n,m}$ in equation 10 for all possible pairs of grid points (n,m)) is 5.5 mm for System A-to-laser tracker instruments and 0.07 mm for System B-to-laser tracker instruments. (Note that the laser tracker is considered noise- and bias-free in this study). The same difference in characteristics of System A and System B is responsible for the overlapping histograms of $\langle RMS_C \rangle$ and $\langle RMS_G \rangle$ in figure 3 (a1, b1) and histogram of $\langle RMS_G \rangle$ shifted right in figure 3c1).

When the triplets of fiducials corresponding to the median values of $\langle RMS_C \rangle$, $\langle RMS_U \rangle$, and $\langle RMS_F \rangle$ were used, the best results, in terms of RMS_U and RMS_C, are obtained for the triplet corresponding to the median of $\langle RMS_F \rangle$ for all three pairs of instruments, System A to System B, System A to laser tracker, and System B to laser tracker (figures 4 and 5 for a–c, and configuration $m = 6$). This observation is surprising, but it reinforces the finding that the selection of fiducials depends on the choice of performance metric. It is interesting that the configuration, $m = 6$, yielding median $\langle RMS_F \rangle$, results in $\langle RMS_C \rangle$ and $\langle RMS_U \rangle$, which are only slightly larger than their smallest values obtained for configuration $m = 1$, as seen in figures 4 and 5.

For a given bias, the distribution of target uncertainty caused by the rotational component of registration transformation is different for different noise levels. In figure 6, the pattern of $\sigma_{m,l}$ distribution calculated from noisy rotations $\boldsymbol{Rj}$ ($j \leq 200$) agree with the pattern of $\gamma_{m,l}$ derived from theoretical prediction,

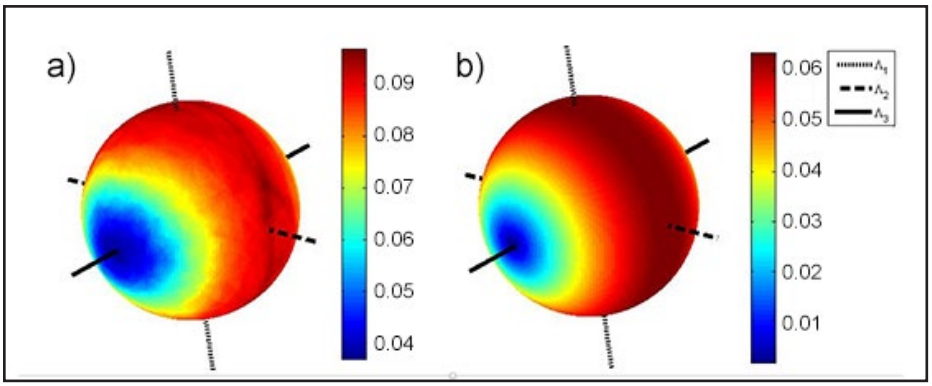

*Figure 6. Angular distribution of the median angle σ in a) and coefficient γ in b) calculated for registration of System A to B using a set of N = 5 fiducials; directions of the three eigenvectors corresponding to the eigenvalues $\Lambda_1 \leq \Lambda_2 \leq \Lambda_3$ of the matrix cov(**q**) are displayed on both graphs from the same view angle; color scale is in* [mrad] *in a) and dimensionless in b)*

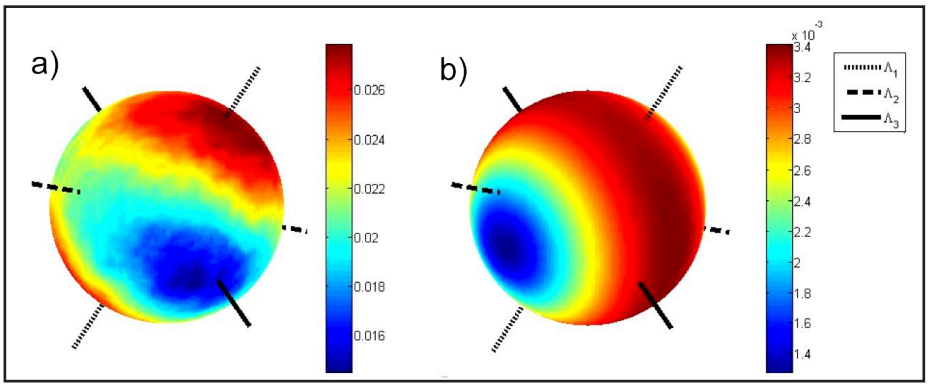

***Figure 7**. Angular distribution of the median angle σ in a) and coefficient γ in b) calculated for registration of System A to laser tracker using a set of N = 5 fiducials; directions of the three eigenvectors corresponding to the eigenvalues $\Lambda_1 \leq \Lambda_2 \leq \Lambda_3$ of the matrix cov(**q**) are displayed on both graphs from the same view angle; color scale is in* [mrad] *in a) and dimensionless in b)*

as seen in equation 17, based on the average fiducial locations $\langle \boldsymbol{X} \rangle_N$ and $\langle \boldsymbol{Y} \rangle_N$. In addition, the eigenvectors of the covariance matrix of the rotational component $cov(\boldsymbol{q})$ are well aligned for both distributions (for example, polar caps of small $\sigma_{m,l}$ and $\gamma_{m,l}$ are centered around the eigenvector corresponding to the largest eigenvalue Λ_3). Data obtained by System A (large bias, small noise) registered to System B (small bias, large noise) were used to create the plots seen in figure 6. Registration of System B to the laser tracker results in distributions very similar to that seen in figure 6. Figure 7 shows the distributions obtained for data acquired by System A and registered to the laser tracker. This time, the pattern of $\sigma_{m,l}$ distribution differs from the pattern of $\gamma_{m,l}$. In addition, the directions of eigenvectors $\{\boldsymbol{u}_1, \boldsymbol{u}_2, \boldsymbol{u}_3\}$ are not aligned with both patterns (polar caps of small $\sigma_{m,l}$ and $\gamma_{m,l}$ are not centered around the poles defined by the eigenvector $\boldsymbol{u}_3$).

In conclusion, it seems that the uncertainty of transformed target points $\langle RMS_U \rangle$ is the best choice for a metric gauging the performance of registration. The metric does not require measurement of targets in the destination frame. The configuration of N fiducials that yields small $\langle RMS_U \rangle$ also yields small target error $\langle RMS_C \rangle$ and $\langle RMS_G \rangle$. However, for measurements with large bias, different configurations of fiducials may have to be selected to minimize either the uncertainty metric $\langle RMS_U \rangle$ or the accuracy metrics $\langle RMS_C \rangle$ $\langle RMS_G \rangle$.

REFERENCES

[1] Sibson, R., "Studies in the Robustness of Multidimensional Scaling: Perturbation Analysis of Classical Scaling," *J. Roy. Statist. Soc. B*, Vol. 41, pp. 217–229, 1979.

[2] Fitzpatrick, J. M., West, J. B., and Maurer, C. R., "Predicting Error in Rigid-Body Point-Based Registration," *IEEE Trans. Medical Imaging*, Vol. 17, pp. 694–702, 1998.

[3] Atuegwu, N. C. and Galloway, R. L., "Sensitivity Analysis of Fiducial Placement on Transorbital Target Registration Error," *Int. J. CARS*, Vol. 2, pp. 397–404, 2008.

[4] Gerard, I. J. and Collins, D. L., "An Analysis of Tracking Error in Image-Guided Neurosurgery," *Int. J. Computer Assisted Radiology and Surgery*, pp. 1–10, 2015.

[5] Shamir, R. R., Joskowicz, L., and Shoshan, Y., "Optimal Landmarks Selection for Minimal Target Registration Error in Image-Guided Neurosurgery," *Proc. SPIE Medical Imaging*, pp. 72612N, 2009.

[6] Shamir, R. R., Joskowicz, L., and Shoshan, Y., "Fiducial Optimization for Minimal Target Registration Error in Image-Guided Neurosurgery," *IEEE Trans. Medical Imaging,* Vol. 31, pp. 725–737, 2012.

[7] Wang, M. and Song, Z., "Improving Target Registration Accuracy in Image-Guided Neurosurgery by Optimizing the Distribution of Fiducial Points," *Int. J. Med. Robotics and Comput. Assist. Surg.*, Vol. 5, pp. 26–31, 2009.

[8] West, J. B., Fitzpatrick, J. M., Toms, S. A., Maurer, C. R., and Maciunas, R. J.. "Fiducial Point Placement and the Accuracy of Point-based, Rigid Body Registration," *Neurosurgery*, Vol. 48, pp. 810–817, 2001.

[9] Danilchenko, A. and Fitzpatrick, J. M., "General Approach to Error Prediction in Point Registration," *Proc. of SPIE Medical Imaging: Visualization, Image-Guided Procedures, and Modeling*, 2010.

[10] Moghari, M. H. and Abolmaesumi, P., "Distribution of Target Registration Error for Anisotropic and Inhomogeneous Fiducial Localization Error," *IEEE Trans. Medical Imaging,* Vol. 28, pp. 799–813, 2009.

[11] Seginer, A., "Rigid-Body Point-Based Registration: The Distribution of the Target Registration Error When the Fiducial Registration Errors Are Given," *Medical Image Analysis,* Vol. 15, pp. 397–413, 2011.

[12] Shamir, R. R. and Joskowicz, L., "Geometrical Analysis of Registration Errors in Point-Based Rigid-Body registration Using Invariants," *Medical Image Analysis*, Vol. 15, pp. 85–95, 2011.

[13] Wiles, A. D., Likholyot, A., Frantz, D. D., and Peters, T. M., "A Statistical Model for Point-Based Target Registration Error With Anisotropic Fiducial Localizer Error," *IEEE Trans. Medical Imaging*, Vol. 27, pp. 378–390, 2008.

[14] Moghari, M. H. and Abolmaesumi, P., "Understanding the Effect of Bias in Fiducial Localization Error on Point-Based Rigid-Body Registration," *IEEE Trans. Medical Imaging*, Vol. 29, pp. 1730–1738, 2010.

[15] Moakher, M., "Means and Averaging in the Group of Rotations," *SIAM J.Matrix Analysis and Applications*, Vol. 24, pp. 1–16, 2002.

[16] Franaszek, M. and Cheok, G. S., "Optimization of Registration Performance Metrics," *NIST IR 8111*, 2016.